

Status of the Zee–Babu model for neutrino mass and possible tests at a like-sign linear collider

Daniel Schmidt,^{1,*} Thomas Schwetz,^{1,2,†} and He Zhang^{1,‡}

¹*Max-Planck-Institut für Kernphysik, Saupfercheckweg 1, 69117 Heidelberg, Germany*

²*Oskar Klein Centre for Cosmoparticle Physics, Department of Physics,
Stockholm University, SE-10691 Stockholm, Sweden*

(Dated: February 11, 2014)

We provide an updated scan of the allowed parameter space of the two-loop Zee–Babu model for neutrino mass. Taking into account most recent experimental data on $\mu \rightarrow e\gamma$ as well as the mixing angle θ_{13} we obtain lower bounds on the masses of the singly and doubly charged scalars of between 1 to 2 TeV, with some dependence on perturbativity and fine-tuning requirements. This makes the scalars difficult to observe at LHC with 14 TeV even with optimistic assumptions on the luminosity, and would require a multi-TeV linear collider to see the scalar resonances. We point out, however, that a sub-TeV linear collider in the like-sign mode may be able to observe lepton flavour violating processes such as $e^-e^- \rightarrow \mu^-\mu^-$ due to contact interactions induced by the doubly charged scalar with masses up to around 10 TeV. We investigate the possibility to distinguish the Zee–Babu model from the Higgs triplet model using such processes.

I. INTRODUCTION

Non-zero neutrino mass requires an extension of the Standard Model (SM). Among the plenitude of possibilities, an attractive way to explain the smallness of neutrino masses is to invoke loop processes, see for instance [1–3] for recent discussions. Then the scale of the new physics responsible for generating neutrino mass can be not too far from the TeV range, which makes those type of models potentially testable at colliders and/or in experiments searching for charged lepton flavour violation (LFV). An economical way of radiative neutrino mass generation is to enlarge the scalar sector of the SM [4, 5]. In this work we concentrate on a particularly simple model of this kind, namely the so-called Zee–Babu model [6–8]. In this model two $SU(2)_L$ singlet scalars are introduced, one singly charged and one doubly charged, and neutrino masses are generated at two-loop level. Through the exchange of heavy scalars, lepton flavour violating processes such as $\mu \rightarrow e\gamma$ can become observable and the new scalars could be accessible at colliders. In particular, the doubly charged scalar may induce very clean like-sign bi-lepton events. Possible connections to Dark Matter within this model have been discussed in [9, 10].

In this paper we provide an update of previous phenomenological studies of the Zee–Babu model [11–14], motivated by various new experimental results relevant for this model. First, precision measurements on reactor neutrinos [15–17] have confirmed that the smallest neutrino mixing angle is non-vanishing and close to the previous upper bound, i.e., $\sin^2 \theta_{13} \simeq 0.023$ [18]. Second, in 2013 the MEG collaboration has provided a new up-

per limit on the LFV process $\mu \rightarrow e\gamma$, with a branching ratio less than 5.7×10^{-13} [19]. We perform a parameter scan of the model taking into account up to date constraints on various LFV and other low-energy processes as well as neutrino oscillation experiments. As a consequence we find that most likely the charged scalars of the Zee–Babu model will be out of reach for the Large Hadron Collider (LHC), including the 14 TeV configuration. Below we comment on the possibilities to observe them indirectly through LFV processes at the proposed International Linear Collider (ILC) in the like-sign mode.

An alternative way to generate neutrino masses is the so-called Higgs triplet model, where an $SU(2)_L$ triplet scalar is introduced, which couples to the lepton doublets and gives rise to a neutrino mass term from the vacuum expectation value of the neutral component [4, 5, 20–22]. If the triplet mass is in the TeV range the doubly charged component could be produced at colliders through the Drell–Yan process, and subsequently decay to lepton pairs, leading to similar signatures as the doubly charged scalar in the Zee–Babu model. If a doubly charged scalar should be found at a collider below the lower bounds in the Zee–Babu model discussed below, it may point towards the Higgs triplet model. In contrast, if no resonance is found the triplet can lead to similar LFV processes at a like-sign electron collider as the Zee–Babu scalar. However, due to the different mechanisms to generate neutrino masses, the specific flavour structure of those processes are distinctive in the two models. We discuss possibilities to distinguish the two models, once such LFV events were observed at a future collider.

The outline of the paper is as follows: In Sec. II, we present the framework and characteristic features of the Zee–Babu model. In Sec. III, we focus on the low-energy processes mediated by the doubly charged scalar and summarize the current constraints on the relevant Yukawa couplings. Numerical analyses on the model parameters are given in Sec. IV. In particular, we illustrate the allowed ranges of the scalar masses. We further dis-

*Electronic address: danielschmidt@t-online.de

†Electronic address: schwetz@fysik.su.se

‡Electronic address: he.zhang@mpi-hd.mpg.de

cuss in Sec. V signatures of the doubly charged scalar at a future linear collider. The discrimination between the Zee–Babu model and the triplet model is investigated in Sec. VI. Finally, in Sec. VII, we summarize our results and conclude.

II. THE ZEE–BABU MODEL

The particle content of the Zee–Babu model is that of the SM extended with two complex $SU(2)_L$ singlet scalars, a singly charged scalar h^+ and a doubly charged scalar k^{++} , which couple to left-handed lepton doublets L and right-handed lepton singlets e , respectively. The contribution to the Lagrangian is

$$\mathcal{L} = f_{ab}\overline{L}_{La}^C i\sigma_2 L_{Lb} h^+ + g_{ab}\overline{e}_a^C e_b k^{++} - \mu h^- h^- k^{++} + \text{h.c.} + V_H, \quad (1)$$

where the scalar potential V_H contains additional couplings among scalar fields. The presence of the trilinear term $\mu k^{++} h^- h^-$ together with the two Yukawa-type terms in the first line of Eq. (1) implies that lepton number is violated.¹ A Majorana mass term for neutrinos is generated via a two-loop diagram, yielding

$$m_{ab}^{(\nu)} = 16\mu f_{ac} m_c g_{cd}^* I_{cd} m_d f_{bd}, \quad (2)$$

where m_c are charged lepton masses and I_{cd} is a two-loop integral [24], which approximates to

$$I_{cd} \approx I = \frac{1}{(16\pi)^2} \frac{1}{M^2} \frac{\pi^2}{3} \tilde{I} \left(\frac{m_k^2}{m_h^2} \right). \quad (3)$$

Here, $M = \max(m_k, m_h)$ and $\tilde{I}(r)$ is a dimensionless function of order unity, see e.g., [13]. Note that the charged scalars couple only to leptons and not at all to hadrons. Therefore, they might contribute to for instance the Fermi constant for leptonic processes, and hence lepton–hadron universality tests provide constraints on the couplings of the scalars, see section III.

Since f is an antisymmetric matrix in flavour space, we have $\det m^{(\nu)} = 0$, and hence one of the light neutrinos is massless. The neutrino mass eigenvalues m_1, m_2, m_3 are obtained by diagonalization of (2) by means of the unitary matrix U :

$$U = R_{23} P_\delta R_{13} P_\delta^{-1} R_{12} P_M, \quad (4)$$

where R_{ij} correspond to the elementary rotations in the $ij = 23, 13$, and 12 planes (parametrized in what follows by three mixing angles, with $c_{ij} \equiv \cos \theta_{ij}$ and $s_{ij} \equiv$

$\sin \theta_{ij}$), and $P_\delta = \text{diag}(1, 1, e^{i\delta})$ and $P_M = \text{diag}(1, e^{i\sigma}, 1)$ contain the Dirac and Majorana CP phases, respectively. Here only one Majorana phase σ is involved, since one neutrino is massless. Depending on the neutrino mass ordering, either m_1 (normal ordering, NO) or m_3 (inverted ordering, IO) is zero. The non-zero neutrino mass states are then determined by the solar and atmospheric mass-squared differences Δm_{21}^2 and $|\Delta m_{31}^2|$, where $\Delta m_{ij}^2 \equiv m_i^2 - m_j^2$.

Using the antisymmetry of f_{ij} (the couplings of h^+), they can be expressed in terms of the neutrino mixing angles [11–13]. In the NO case, we have

$$\frac{f_{e\tau}}{f_{\mu\tau}} = \frac{s_{12}c_{23}}{c_{12}c_{13}} + \frac{s_{13}s_{23}}{c_{13}} e^{-i\delta}, \quad (5)$$

$$\frac{f_{e\mu}}{f_{\mu\tau}} = \frac{s_{12}s_{23}}{c_{12}c_{13}} - \frac{s_{13}c_{23}}{c_{13}} e^{-i\delta}. \quad (6)$$

Since s_{13} is relatively small compared to the other mixing angles, we can neglect the second terms in the above expressions, and obtain the approximate relation

$$f_{e\mu} \simeq f_{e\tau} \simeq f_{\mu\tau}/2 \quad (7)$$

by assuming $s_{12}^2 \simeq 1/3$ and $s_{23}^2 \simeq 1/2$. For the IO case, the two non-trivial equations are

$$\frac{f_{e\tau}}{f_{\mu\tau}} = -\frac{s_{23}c_{13}}{s_{13}} e^{-i\delta}, \quad (8)$$

$$\frac{f_{e\mu}}{f_{\mu\tau}} = \frac{c_{13}c_{23}}{s_{13}} e^{-i\delta}, \quad (9)$$

which imply

$$\left| \frac{f_{e\tau}}{f_{e\mu}} \right| = \tan \theta_{23} \simeq 1 \quad \text{and} \quad |f_{\mu\tau}| \simeq |f_{e\tau}| \frac{s_{13}}{s_{23}}. \quad (10)$$

Using Eq. (2), the Yukawa couplings g_{ab} of the doubly charged scalar are related to the neutrino mass matrix elements as

$$\begin{aligned} m_{22}^{(\nu)} &= \zeta (f_{\mu\tau}^2 \omega_{\tau\tau} - 2f_{e\mu} f_{\mu\tau} \omega_{e\tau} + f_{e\mu}^2 \omega_{ee}) \\ m_{23}^{(\nu)} &= \zeta (f_{\mu\tau} f_{e\mu} \omega_{e\mu} + f_{e\tau} f_{e\mu} \omega_{ee} - f_{\mu\tau}^2 \omega_{\mu\tau} - f_{\mu\tau} f_{e\tau} \omega_{e\tau}) \\ m_{33}^{(\nu)} &= \zeta (f_{\mu\tau}^2 \omega_{\mu\mu} + 2f_{e\tau} f_{\mu\tau} \omega_{e\mu} + f_{e\tau}^2 \omega_{ee}) \end{aligned} \quad (11)$$

where $\omega_{ab} = m_a g_{ab}^* m_b$ (no sum) with m_a being the charged lepton masses and $\zeta \propto \mu$ is a numerical factor stemming from the loop function.

III. EXPERIMENTAL CONSTRAINTS

The experimental bounds on the Zee–Babu model mainly come from lepton flavour violating processes at low-energy scales mediated by the heavy scalars, and the universality of weak interactions. In this section, we summarize the relevant low-energy scale experimental limits on the Zee–Babu model.

¹ In the original Zee–Babu model as displayed in Eq. (1), the trilinear term which violates lepton number by two units has to be introduced “by hand”. It is possible to have instead a lepton number conserving interaction which generates the μ term by spontaneous symmetry breaking, see e.g., [9, 23].

- Lepton flavour violating decays $\ell_a^- \rightarrow \ell_b^+ \ell_c^- \ell_d^-$, which are mediated by the doubly charged scalar k^{++} at tree level. The branching ratio is given by $\text{BR}(\ell_a^- \rightarrow \ell_b^+ \ell_c^- \ell_d^-) = R_a^{bcd} \times \text{BR}(\ell_a^- \rightarrow \ell_b^- \nu \bar{\nu})$ with

$$R_a^{bcd} = \frac{1}{2(1 + \delta_{cd})} \left| \frac{g_{ab} g_{cd}^*}{G_F m_k^2} \right|^2. \quad (12)$$

- Universality in $\ell_a^- \rightarrow \ell_b^- \nu \bar{\nu}$ decays: The Fermi coupling constant measured in muon and tau decays obtains corrections from the exchange of h^+ , i.e.,

$$\left[\frac{G_{\tau \rightarrow \mu}}{G_{\tau \rightarrow e}} \right]^2 \simeq 1 + \frac{\sqrt{2}}{G_F m_h^2} \left(|f_{\mu\tau}|^2 - |f_{e\tau}|^2 \right). \quad (13)$$

Furthermore, by assuming the unitarity of the CKM matrix, one can test the universality of the couplings in hadronic and leptonic decays, which gives

$$|V_{ud}|^2 + |V_{us}|^2 + |V_{ub}|^2 \simeq 1 - \frac{\sqrt{2}}{G_F m_h^2} |f_{e\mu}|^2. \quad (14)$$

In Eqs. (13) and (14) G_F is the Fermi coupling constant as given by the SM contribution. We show only the leading terms in the couplings f_{ab} , which emerge from the interference of the SM diagram with the ones mediated by the Zee–Babu scalars.

- Rare lepton decays: $\ell_a^- \rightarrow \ell_b^- \gamma$ (for $a \neq b$) can be mediated at one-loop level by both k^{++} and h^+ , and the branching ratios read $\text{BR}(\ell_a^- \rightarrow \ell_b^- \gamma) = R_a^{b\gamma} \times \text{BR}(\ell_a^- \rightarrow \ell_b^- \nu \bar{\nu})$, where

$$R_a^{b\gamma} = \frac{\alpha}{48\pi} \left(\left| \frac{(f^\dagger f)_{ab}}{G_F m_h^2} \right|^2 + 16 \left| \frac{(g^\dagger g)_{ab}}{G_F m_k^2} \right|^2 \right). \quad (15)$$

- Muonium to antimuonium conversion through the exchange of k^{++} : The process $\mu^+ e^- \rightarrow \mu^- e^+$ is well bounded experimentally, leading to constraints on the effective coupling related to the following four-fermion operator

$$G_{M\bar{M}} = -\frac{\sqrt{2}}{8} \frac{g_{ee} g_{\mu\mu}^*}{m_k^2}. \quad (16)$$

- Muon and electron anomalous magnetic moments: $a = (g - 2)/2$ obtains addition contributions δa from both h^+ and k^{++} , with

$$\delta a_a = -\frac{m_a^2}{24\pi^2} \left(\frac{(f^\dagger f)_{aa}}{m_h^2} + 4 \frac{(g^\dagger g)_{aa}}{m_k^2} \right), \quad (17)$$

where $a = e, \mu$. The bound from δa_e is very weak (only relevant for scalar masses above 10^3 TeV) and therefore we include only the constraint from δa_μ .

- $\mu - e$ conversion in nuclei: The loops which mediate the decays $\mu^- \rightarrow e^- \gamma$ generate an effective $\mu e \gamma$ vertex which induces $\mu - e$ conversion in nuclei. Using the result from [25] we obtain

$$\text{CR}(\mu N \rightarrow e N) \simeq \frac{2e^2 G_F^2}{\Gamma_{\text{capt}}} \times \left(\left| A_R^h D + e A_L^h V^{(p)} \right|^2 + \left| A_R^k D + e A_L^k V^{(p)} \right|^2 \right), \quad (18)$$

where D and $V^{(p)}$ represent overlap integrals of the muon and electron wave functions. The form factors are given by the same expressions as in the case of the Higgs triplet model [26]

$$\begin{aligned} A_R^h &= -\frac{(f^\dagger f)_{e\mu}}{768\sqrt{2}\pi^2 G_F m_h^2}, \\ A_R^k &= -\frac{(g^\dagger g)_{e\mu}}{48\sqrt{2}\pi^2 G_F m_k^2}, \\ A_L^h &= -\frac{(f^\dagger f)_{e\mu}}{144\sqrt{2}\pi^2 G_F m_h^2}, \\ A_L^k &= -\sum_{a=e,\mu,\tau} \frac{g_{ae}^* g_{a\mu}}{6\sqrt{2}\pi^2 G_F m_k^2} F\left(\frac{-q^2}{m_k^2}, \frac{m_a^2}{m_k^2}\right), \end{aligned} \quad (19)$$

where the loop function is [27]

$$\begin{aligned} F(x, y) &= \frac{4y}{x} + \log(y) + \left(1 - \frac{2y}{x}\right) \\ &\times \sqrt{1 + \frac{4y}{x}} \log \frac{\sqrt{x+4y} + \sqrt{x}}{\sqrt{x+4y} - \sqrt{x}}. \end{aligned} \quad (20)$$

Note that in the Higgs triplet model both the singly and doubly charged scalars couple to left-handed leptons (since both are components of the same $SU(2)$ triplet field), whereas in the Zee–Babu model h couples to left-handed and k^{++} couples to right-handed leptons, see Eq. (1). Therefore, the amplitudes for singly and doubly charged scalar mediated processes do not interfere in the case of the Zee–Babu model, whereas they do in the case of the Higgs triplet model [25].

We summarize in Table I the low-energy experimental constraints used in our analysis. One can observe that lepton flavour violating processes set more stringent bounds on the Yukawa couplings, in particular the $\mu \rightarrow e\gamma$ and $\mu \rightarrow 3e$ decays. The later process could however be suppressed in the Zee–Babu model if g_{ee} or $g_{e\mu}$ is vanishing, which is possible while still obtaining a valid neutrino mass matrix. The $\mu \rightarrow e\gamma$ decay is mediated by both singly and doubly charged scalars, and is proportional to both Yukawa couplings f and g , which cannot vanish simultaneously. Therefore, the most stringent constraint on the Zee–Babu model stems from the $\mu \rightarrow e\gamma$ decay.

Constraint	Ref.	Bound (90% C.L.)
$\sum_{q=d,s,b} V_{uq} ^2$	0.99990 ± 0.0006 [28]	$ f_{e\mu} ^2 < 0.014 \left(\frac{m_h}{\text{TeV}}\right)^2$
$\mu - e$ universality	$\frac{G_{\tau \rightarrow \mu}}{G_{\tau \rightarrow e}} = 1.0001 \pm 0.0020$ [28]	$ f_{\mu\tau} ^2 - f_{e\tau} ^2 < 0.05 \left(\frac{m_h}{\text{TeV}}\right)^2$
$\mu - \tau$ universality	$\frac{G_{\tau \rightarrow e}}{G_{\mu \rightarrow e}} = 1.0004 \pm 0.0022$ [28]	$ f_{e\tau} ^2 - f_{e\mu} ^2 < 0.06 \left(\frac{m_h}{\text{TeV}}\right)^2$
$e - \tau$ universality	$\frac{G_{\tau \rightarrow \mu}}{G_{\mu \rightarrow e}} = 1.0004 \pm 0.0023$ [28]	$ f_{\mu\tau} ^2 - f_{e\mu} ^2 < 0.06 \left(\frac{m_h}{\text{TeV}}\right)^2$
δa_μ	$(28.7 \pm 80) \times 10^{-10}$ [28, 29]	$r(f_{e\mu} ^2 + f_{\mu\tau} ^2) + 4(g_{e\mu} ^2 + g_{\mu\mu} ^2 + g_{\mu\tau} ^2) < 3.4 \left(\frac{m_k}{\text{TeV}}\right)^2$
$\mu^- \rightarrow e^+ e^- e^-$	BR < 1.0×10^{-12} [30]	$ g_{e\mu} g_{ee}^* < 2.3 \times 10^{-5} \left(\frac{m_k}{\text{TeV}}\right)^2$
$\tau^- \rightarrow e^+ e^- e^-$	BR < 2.7×10^{-8} [31]	$ g_{e\tau} g_{ee}^* < 0.009 \left(\frac{m_k}{\text{TeV}}\right)^2$
$\tau^- \rightarrow e^+ e^- \mu^-$	BR < 1.8×10^{-8} [31]	$ g_{e\tau} g_{e\mu}^* < 0.005 \left(\frac{m_k}{\text{TeV}}\right)^2$
$\tau^- \rightarrow e^+ \mu^- \mu^-$	BR < 1.7×10^{-8} [31]	$ g_{e\tau} g_{\mu\mu}^* < 0.007 \left(\frac{m_k}{\text{TeV}}\right)^2$
$\tau^- \rightarrow \mu^+ e^- e^-$	BR < 1.5×10^{-8} [31]	$ g_{\mu\tau} g_{ee}^* < 0.007 \left(\frac{m_k}{\text{TeV}}\right)^2$
$\tau^- \rightarrow \mu^+ e^- \mu^-$	BR < 2.7×10^{-8} [31]	$ g_{\mu\tau} g_{e\mu}^* < 0.006 \left(\frac{m_k}{\text{TeV}}\right)^2$
$\tau^- \rightarrow \mu^+ \mu^- \mu^-$	BR < 2.1×10^{-8} [31]	$ g_{\mu\tau} g_{\mu\mu}^* < 0.008 \left(\frac{m_k}{\text{TeV}}\right)^2$
$\mu \rightarrow e\gamma$	BR < 5.7×10^{-13} [19]	$r^2 f_{e\tau}^* f_{\mu\tau} ^2 + 16 g_{e\alpha}^* g_{\alpha\mu} ^2 < 1.6 \times 10^{-6} \left(\frac{m_k}{\text{TeV}}\right)^4$
$\tau \rightarrow e\gamma$	BR < 3.3×10^{-8} [32]	$r^2 f_{e\mu}^* f_{\mu\tau} ^2 + 16 g_{e\alpha}^* g_{\alpha\tau} ^2 < 0.52 \left(\frac{m_k}{\text{TeV}}\right)^4$
$\tau \rightarrow \mu\gamma$	BR < 4.5×10^{-8} [32]	$r^2 f_{e\mu}^* f_{e\tau} ^2 + 16 g_{\mu\alpha}^* g_{\alpha\tau} ^2 < 0.71 \left(\frac{m_k}{\text{TeV}}\right)^4$
$\mu \leftrightarrow e$ conversion	CR < 7.0×10^{-13} [33]	see Eq. (19)
$\mu^+ e^- \rightarrow \mu^- e^+$	$G_{MM} < 3 \times 10^{-3} G_F$ [28]	$ g_{ee} g_{\mu\mu}^* < 0.2 \left(\frac{m_k}{\text{TeV}}\right)^2$

TABLE I: Summary of experimental constraints and the corresponding bounds on the Yukawa couplings. Here $r = m_k^2/m_h^2$, and $g_{e\alpha}^* g_{\alpha\mu} = g_{ee}^* g_{e\mu} + g_{e\mu}^* g_{\mu\mu} + g_{e\tau}^* g_{\tau\mu}$ and so on.

IV. NUMERICAL ANALYSIS

We perform a scan of the Zee–Babu model parameters confronting the experimental data in order to obtain constraints on the scalar masses. The independent parameters can be chosen as: three leptonic mixing angles; Dirac and Majorana phases δ , σ ; the Yukawa couplings g_{ee} , $g_{e\mu}$, $g_{e\tau}$, $f_{\mu\tau}$; scalar masses m_k , m_h ; and the μ parameter in the scalar potential. Neutrino masses are fixed to the values set by the best fit mass-squared differences [18]. Then the remaining Yukawa couplings g_{ab} and f_{ab} are fixed by Eqs. (5), (6), (8), (9), (11). For simplicity we fix the mixing angles to the values [18] $\sin^2 \theta_{12} = 0.30$, $\sin^2 \theta_{23} = 0.41$, $\sin^2 \theta_{13} = 0.023$. The remaining parameters are scanned in the following ranges:

$$\begin{aligned}
\delta &= [0, 2\pi) \\
\sigma &= [0, \pi) \\
|g_{ee}|, |g_{e\mu}|, |g_{e\tau}|, f_{\mu\tau} &= [0, \kappa) \\
\mu &= [0, \lambda \times \min(m_k, m_h)) \quad (21)
\end{aligned}$$

where κ parametrizes the requirement of perturbativity of Yukawa couplings. If not stated otherwise we take $\kappa = 1$. For the tri-linear term, the μ parameter induces loop corrections to the scalar masses as $\delta m_{k,h}^2 \sim \mu^2/(4\pi)^2$. In the absence of fine-tuning the correction should be smaller than the tree-level masses, which leads to the constraint $\mu \ll 4\pi m_{k,h}$. Henceforth, we parameterize this requirement by a parameter λ , see Eq. (21). The phases of g_{ee} , $g_{e\mu}$, $g_{e\tau}$ are chosen randomly, whereas $f_{\mu\tau}$ can be taken real without loss of generality. For a given set of the parameters in Eq. (21) we check if all other

values for g_{ab} and f_{ab} are less than κ ; if not then the point is discarded. If the perturbativity constraint is fulfilled we compare the model predictions to the experimental data with a χ^2 function

$$\chi_i^2 = \frac{(\rho_i - \rho_i^0)^2}{\sigma_i^2}, \quad (22)$$

where ρ_i^0 represents the data of the i th experimental observable, σ_i the corresponding 1σ absolute error, and ρ_i the prediction of the model. The index $i = 1, \dots, 17$ runs over the 17 experimental observables given in Table I. In case of upper bounds we set $\rho_i^0 = 0$ and use the 1σ upper bound for σ_i . In order to identify the allowed regions in parameter space we proceed as follows. For a given point in parameter space we consider the maximum χ_i^2 of all data points:

$$\chi_{\max}^2 = \max_i \chi_i^2. \quad (23)$$

If $\chi_{\max}^2 \leq 4$ is fulfilled we keep the point, otherwise it is discarded. In that way we make sure that all data points are fitted within 2 standard deviations. Let us stress that we do not adopt any particular statistical interpretation of the resulting regions in parameter space in terms of confidence regions, apart from the above statement that all constraints are satisfied within 2σ .

From Eqs. (11) one can see that the contribution of the couplings g_{ee} ($g_{e\mu}$, $g_{e\tau}$) is suppressed by two powers (one power) of the electron mass. Indeed, we find always viable solutions for $g_{ee} = g_{e\mu} = g_{e\tau} = 0$. However, we do take into account finite values in our scan in order to allow for sub-leading effects induced by those couplings.

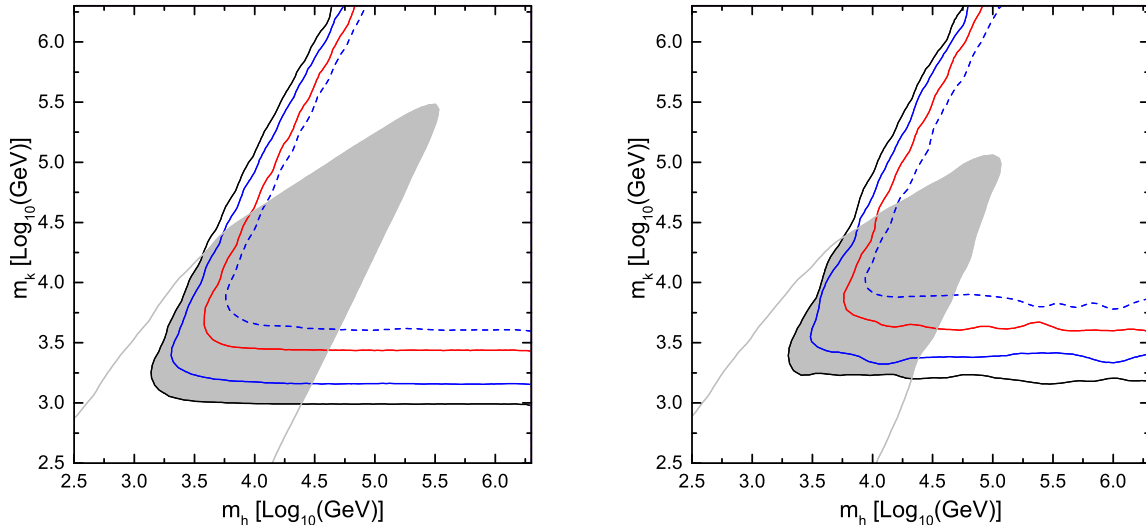


FIG. 1: The shadowed regions correspond to allowed ranges of the scalar masses for the normal mass ordering (left panel) and the inverted mass ordering (right panel) by requiring $\chi_{\max}^2 < 4$ and imposing the perturbativity criterion $\lambda = \kappa = 1$. The black, blue, and red curves correspond to lower limits on the scalar masses obtained from the experimental data by requiring $\chi_{\max}^2 < 4$ but without the κ constraint. The black curve corresponds to the current experimental bounds. The blue solid and blue dashed curves show the exclusion regions from the expected $\mu - e$ conversion constraint $\text{CR}(\mu\text{Al} \rightarrow e\text{Al}) < 6 \times 10^{-17}$ and $\text{CR}(\mu\text{Al} \rightarrow e\text{Al}) < 10^{-18}$, respectively. The red line is given by assuming $\text{BR}(\mu \rightarrow e\gamma) < 10^{-14}$. Furthermore, gray curves delimit the region allowed by perturbativity without requiring that the experimental constraints are respected.

The allowed ranges of scalars masses are illustrated in Fig. 1 for both normal and inverted mass orderings. For scalar masses within the shadowed regions all the constraints are satisfied in the sense of $\chi_{\max}^2 < 4$ and $\lambda = \kappa = 1$ as explained above. We observe that the parameter space of the model is closed, however, allowing for $\lambda \sim \kappa \sim 1$ scalar masses up to $\mathcal{O}(100 \text{ TeV})$ are possible. If we allow for some fine-tuning in the scalar potential by setting the parameter λ to 4π , the upper bound on the scalar masses will be larger than 10^3 TeV (see Fig. 2 below). Note however, that large scalar masses require Yukawa couplings close to the perturbativity limit. If Yukawa couplings assume values $g_{\alpha\beta}, f_{\alpha\beta} \ll 1$ the scalar masses get pushed towards lower values. The lower bound on the scalar masses (black curve) is dominated by the observables from Tab. I, most importantly from the MEG bound on $\mu \rightarrow e\gamma$. We obtain the following lower bounds by requiring that all constraints are satisfied at 2σ :

$$\begin{aligned} m_k > 1.3 \text{ TeV}, \quad m_h > 1.3 \text{ TeV} \quad (\text{NO}) \\ m_k > 1.9 \text{ TeV}, \quad m_h > 2.0 \text{ TeV} \quad (\text{IO}) \end{aligned} \quad (\lambda = 1). \quad (24)$$

Note that the lowest possible value for the doubly charged scalar k occurs for relatively large values of singly charged scalar mass and depends also on the perturbativity/fine-tuning conditions. In deriving the bounds we have assumed $\lambda = 1$. If we allow values for the tri-linear coupling μ larger than the scalar masses (amounting to some

fine-tuning in the scalar potential) the lower bounds on the Zee-Babu scalars can be relaxed. For example, we show the mass ranges in Fig. 2 by taking a relatively large constraint $\lambda = 5$. One can see that the lower bounds on the scalar masses reduce to

$$\begin{aligned} m_k > 0.5 \text{ TeV}, \quad m_h > 0.6 \text{ TeV} \quad (\text{NO}) \\ m_k > 0.8 \text{ TeV}, \quad m_h > 1.0 \text{ TeV} \quad (\text{IO}) \end{aligned} \quad (\lambda = 5). \quad (25)$$

The bounds for IO can be further weakened by fine tuning of the complex phases $\delta \approx \pi$ and $\sigma \approx \pi/2$, leading to a cancellation between different terms in Eq. (11). By performing a dedicated search with phases constrained to be very close to those special values we find that the IO bounds for m_k and m_h in Eq. (24) reduce to around 1.0 and 1.1 TeV, respectively. Let us also stress that our bounds are obtained by a random parameter scan, throwing 10^5 points for a given choice of m_k and m_h , out of which only a fraction passes our perturbativity requirement. With such a method fine tuned solutions as the one mentioned above might be missed. In this sense our bounds for the scalar masses hold for “generic” values of the parameters.

There are several future projects aiming for improving significantly the bound on $\mu - e$ conversion by about 4 to 5 orders of magnitude compared to the current limit [33], for instance the Mu2e [34, 35] and COMET [36] experiments aim at sensitivities of order 10^{-16} , whereas the target sensitivity of the PRISM project [37] is even

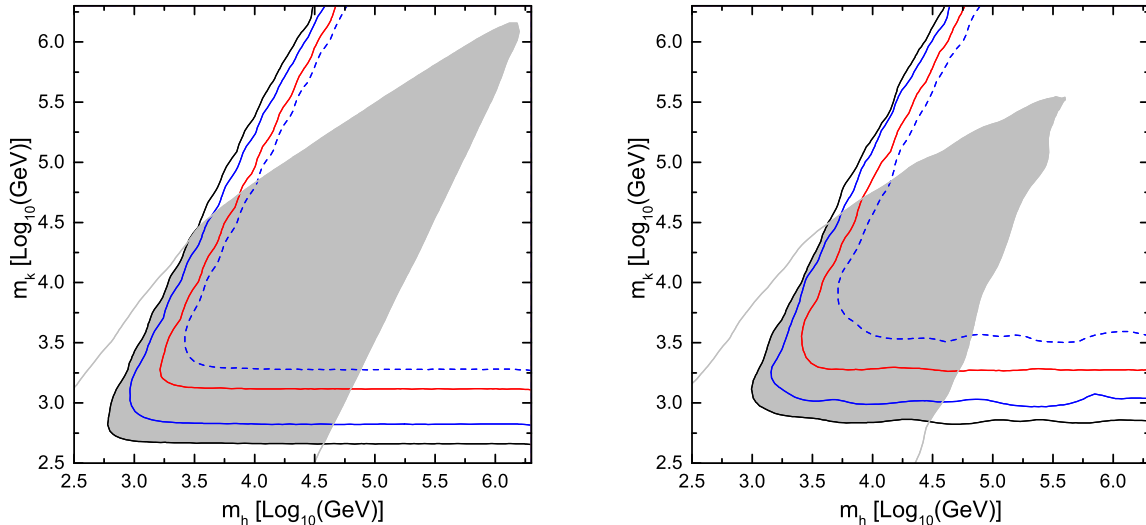


FIG. 2: The same as Fig. 1 with $\lambda = 5$, i.e., allowing for a tri-linear coupling μ larger than the scalar masses, see Eq. (21).

of order 10^{-18} . Furthermore, an upgrade program is underway for the MEG experiment aiming at a sensitivity improvement of a further order of magnitude [19]. We thus also show in Figs. 1 and 2 with colored contours the future experimental constraints on the charged scalars. Those improved constraints on LFV (if no positive signal is found) will further push up the lower bounds on the scalar masses of about 1 order of magnitude. However, it is still difficult to entirely rule out the Zee–Babu model, no matter for the normal or inverted mass ordering (depending on the perturbativity requirements).

It should be noticed that our analysis is based on the latest measurement on the smallest mixing angle θ_{13} , which is indeed very crucial for the IO case. For illustration purposes, we show in Fig. 3 also a similar numerical analysis but using $s_{13}^2 = 0.001$ (which is by now excluded by oscillation data). In this case, there is no overlap between the perturbativity contours and the experimental contours, indicating that the Zee–Babu model is incompatible with the inverted mass ordering if θ_{13} is very small. In other words, if the neutrino mass ordering is inverted, the Zee–Babu model can then be viewed as a natural candidate for predicting sizeable θ_{13} , see e.g., [13]. Such a feature is also manifest in Eqs. (8) and (9), showing that both, $f_{e\mu}$ and $f_{e\tau}$ are inversely proportional to s_{13} , and therefore a too small s_{13} may blow up Yukawa couplings resulting in a conflict with lepton flavour violation constraints. Conversely, there is no inverse dependence on θ_{13} in the case of normal mass ordering, c.f. Eqs. (5) and (6), and thus the choice of θ_{13} has no important impact on the Zee–Babu model parameters. We have checked this point numerically by choosing different values for θ_{13} , and they all give almost the same scalar mass ranges for normal ordering.

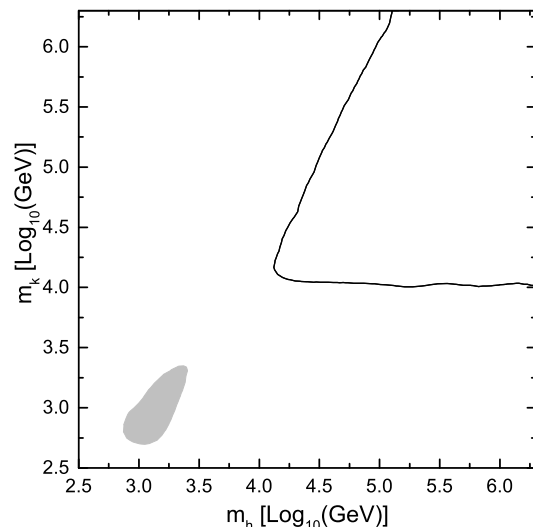


FIG. 3: Allowed ranges of the scalar masses for the inverted mass ordering for $s_{13} = 0.001$ by requiring $\chi_{\max}^2 < 4$. The black curve corresponds to the current experimental bounds. The shadowed area contour is allowed by the perturbativity criterion $\lambda = \kappa = 1$ (without imposing the constraints from Tab. I).

As discussed above, present data pushes the masses of the singly and doubly charged scalars of the Zee–Babu model above the TeV, see Eq. (24). This makes the direct production at colliders difficult. The production cross

sections of the Zee–Babu scalars have been calculated in [11–13], for recent work on di-leptons in general see e.g., [38, 39]. ATLAS [40] and CMS [41] have searched for doubly charged scalars decaying predominantly into muons and/or electrons based on approximately 5 fb^{-1} at $\sqrt{s} = 7 \text{ TeV}$, obtaining lower bounds on their mass of around 400 GeV. The results of [13] show that for the Zee–Babu doubly charged scalar with masses $m_k = 0.5, 1, 1.5 \text{ TeV}$ of order 300, 10, 1 events are expected at LHC for 300 fb^{-1} at $\sqrt{s} = 14 \text{ TeV}$, respectively, assuming 100% branching fraction of k^{++} into leptons. Given the constraints on the masses derived above this implies that most likely the Zee–Babu scalars will not be observable at LHC, unless some degree of fine-tuning is accepted and the relaxed bounds of Eq. (25) apply. In that case, future experiments for LFV would also observe a positive signal, see Fig. 2.

V. TESTS AT AN e^-e^- COLLIDER

At a possible future e^+e^- linear collider the scalars can be pair-produced by photon and Z exchange: $e^+e^- \rightarrow k^{++}k^{--}$. Obviously this requires center of mass energies of $\sqrt{s} > 2m_{k,h}$, which in view of the bounds in Eq. (24) seems not realistic in the foreseeable future. However, a linear collider may also be operated in the like-sign mode. This offers a new window to search for LFV processes within the context of the Zee–Babu model for scalar masses up to $\sim 10 \text{ TeV}$.

The possibility to test bi-leptons at a like-sign electron collider has been considered since long time, see Refs. [42–49] for an incomplete list of references. Lots of work has been devoted to the search for lepton number violating reactions $e^-e^- \rightarrow W^-W^-$ in the context of Higgs triplet models. In the Zee–Babu model this process is not allowed at tree level. However, lepton flavour violating (but lepton number conserving) reactions such as $e^-e^- \rightarrow \ell_\alpha^- \ell_\beta^-$ mediated by k^{--} at tree level may be observable.

The cross section for the process $e^-e^- \rightarrow \ell_\alpha^- \ell_\beta^-$ for $(\alpha\beta) \neq (ee)$ is given by

$$\sigma(ee \rightarrow \alpha\beta) = \frac{S|g_{ee}g_{\alpha\beta}|^2}{4\pi(1 + \delta_{\alpha\beta})} \frac{s}{(s - m_k^2)^2 + m_k^2\Gamma_k^2}, \quad (26)$$

where Γ_k is the width of the doubly charged scalar, and $S = (1 + P_1)(1 + P_2)$ the polarization factor of the incoming electron beams. First, we note that this process is proportional to $|g_{ee}|^2$. As mentioned above, this coupling is not determined by neutrino data and in principle it could be zero. Hence, no signal can be predicted. On the other hand, also the upper bound on this coupling is rather weak and therefore a sizeable cross section would be possible in principle. The upper limit on the cross section as a function of the center of mass energy is shown in Fig. 4 for unpolarized beams ($S = 1$). For center of mass energies of $\sqrt{s} > m_k$ a sharp resonance can be observed,

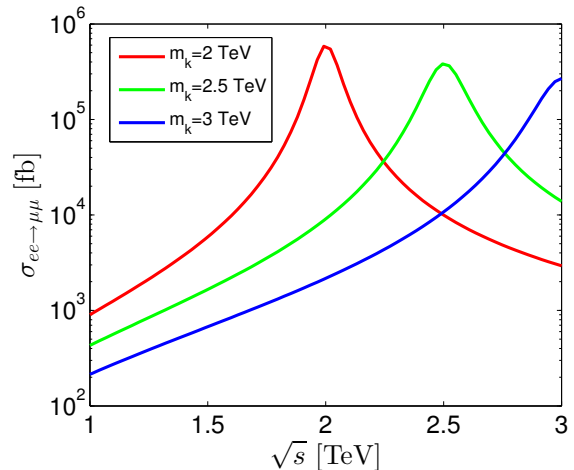


FIG. 4: Upper limit on the cross section $\sigma(e^-e^- \rightarrow \mu^-\mu^-)$ as a function of the center of mass energy \sqrt{s} for normal neutrino mass ordering for doubly charged scalar masses of 2, 2.5, and 3 TeV.

leading to very large cross sections in excess of 100 pb, allowing for the direct discovery of the doubly charged scalar. In view of the bounds from Eq. (24), this will require a multi-TeV collider. However, for lower center of mass energies, one may still expect visible cross sections, corresponding to contact interactions mediated by the heavy scalar.

We show in Fig. 5 the upper limits on the cross section as a function of the scalar mass for center of mass energies $\sqrt{s} = 500, 700, 1000 \text{ GeV}$ (solid curves). For a total luminosity of 50 fb^{-1} , more than a few tens of events can be expected for a scalar mass $m_k \lesssim 10 \text{ TeV}$. Also note that, for a smaller m_k , the reduction of the cross section for IO is due to the LFV constraints. While such a signature will not allow for the direct discovery of the doubly charged scalar via a resonance, it would provide indirect evidence for a doubly charged particle. The flavour and chirality structure of the LFV processes $e^-e^- \rightarrow \alpha^-\beta^-$ would offer additional consistency checks with the Zee–Babu model, as we are going to discuss in the next section.

VI. DISTINGUISHING THE ZEE–BABU AND THE HIGGS TRIPLET MODEL

Once a signal induced by a doubly charged scalar is found at a collider experiment, an interesting task will be to identify the underlying model and establish the connection to the mechanism to generate neutrino mass. Here we focus on ways to distinguish the Zee–Babu model from the Higgs triplet model, which also predicts the existence of a doubly charged scalar particle. The leptonic part of the Lagrangian contains the term

$$\mathcal{L}_\Delta = h_{\alpha\beta} \bar{L}_\alpha^c i\tau_2 \Delta L_\beta + \text{H.c.}, \quad (27)$$

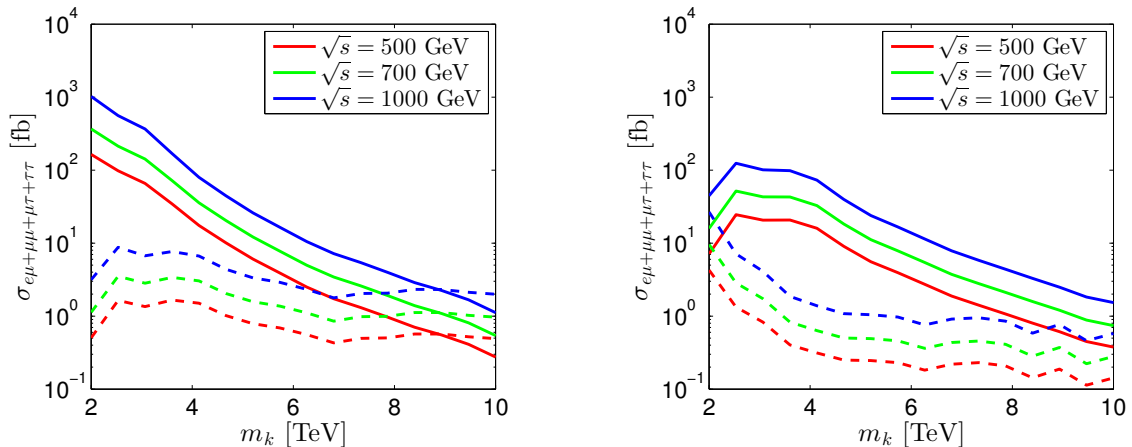


FIG. 5: Upper limits on the sum of the cross sections $\sigma(e^-e^- \rightarrow \mu^-\mu^-) + \sigma(e^-e^- \rightarrow \mu^-e^-) + \sigma(e^-e^- \rightarrow \mu^-\tau^-) + \sigma(e^-e^- \rightarrow \tau^-\tau^-)$ as a function of the doubly charged scalar mass for center of mass energies $\sqrt{s} = 500, 700, 1000$ GeV. Solid curves correspond to the Zee–Babu model, where $\sigma(e^-e^- \rightarrow \mu^-\mu^-)$ dominates the sum. Dashed curves correspond to the Higgs triplet model, where the lightest neutrino mass is allowed to vary between 0 and 0.2 eV. The left (right) panel corresponds to normal (inverted) neutrino mass ordering.

where $h_{\alpha\beta}$ is a symmetric Yukawa coupling matrix and Δ is a 2×2 representation of the $SU(2)_L$ Higgs triplet containing neutral, singly charged, and doubly charged components. Neutrino masses are generated by the vacuum expectation value (VEV) of the neutral component. Hence the Yukawa couplings $h_{\alpha\beta}$ are directly proportional to the neutrino mass matrix. Below we outline a few possibilities to distinguish the Zee–Babu model from the Higgs triplet model.

A. Signatures at a like-sign linear collider

Similar as in the Zee–Babu model, also in the Higgs triplet model the process $e^-e^- \rightarrow \alpha^-\beta^-$ is possible at a like-sign linear collider with a cross section in complete analogy to Eq. (26) (see e.g., [49]), with the coupling $g_{\alpha\beta}$ replaced by $h_{\alpha\beta}$ and $S \rightarrow (1 - P_1)(1 - P_2)$, taking into account that for the triplet left-handed leptons couple to the doubly charged scalar, in contrast to the right-handed coupling in the Zee–Babu model. In Fig. 5 we compare the maximum obtainable value for the sum of the cross sections for lepton flavour violating processes for the Higgs triplet model (dashed) to the one for the Zee–Babu model (solid). For the Higgs triplet model, the lightest neutrino mass is not necessarily vanishing, therefore, in Fig. 5 we vary its value between zero and 0.2 eV. The VEV of the triplet is varied between 0.1 eV and 1 keV, where the largest cross sections are obtained for small values, since in this case Yukawa couplings are largest. The two Majorana phases are allowed to vary freely between 0 and π , and the Dirac phase δ between 0 and 2π . As for the Zee–Babu model, we use the current experimental bounds, i.e., the same constraints as for the black curves in Fig. 1. For the triplet model we

include the constraints from $\mu \rightarrow e\gamma$, $\mu \rightarrow 3e$, muonium–antimuonium conversion, and $\mu - e$ conversion in nuclei. The corresponding expression can be found for instance in [25–27]. We find cross sections of order 1 fb, and those results suggest that with integrated luminosities of $\gtrsim 10 \text{ fb}^{-1}$ such lepton flavour violating processes can also be expected to be observed in the Higgs triplet model. Note that here we are in the regime of \sqrt{s} much smaller than the mass of the doubly charged scalar, which implies that no resonance is seen and hence the mass cannot be determined. Furthermore, we stress again that those curves are upper bounds, and in particular, for the Zee–Babu model the cross section can be easily reduced by adjusting g_{ee} which is not bounded from below. Therefore the size of the cross section by itself does not allow to distinguish the two models.

Before we discuss the possibility to use the flavour structure to distinguish the models, let us mention the importance of the lightest neutrino mass in the case of the triplet model. Since the cross section for $e^-e^- \rightarrow \alpha^-\beta^-$ is proportional to $h_{ee} \propto m_{ee}^{(\nu)}$ the value of the lightest neutrino mass is important, especially for normal mass ordering, where the possible size of $m_{ee}^{(\nu)}$ depends strongly on m_1 . In Fig. 6 we show the maximum obtainable value for the sum of the cross sections for lepton flavour violating processes as a function of the lightest neutrino mass. We observe that for strongly hierarchical spectrum with normal ordering the cross section becomes very small. Hence, establishing normal mass ordering by oscillation experiments plus setting an upper bound on the lightest neutrino mass below 0.05 eV (for instance by cosmology or neutrinoless double beta decay) would make the signal in the triplet model very small. In that case a sizeable signal at the like-sign collider would favour the Zee–Babu

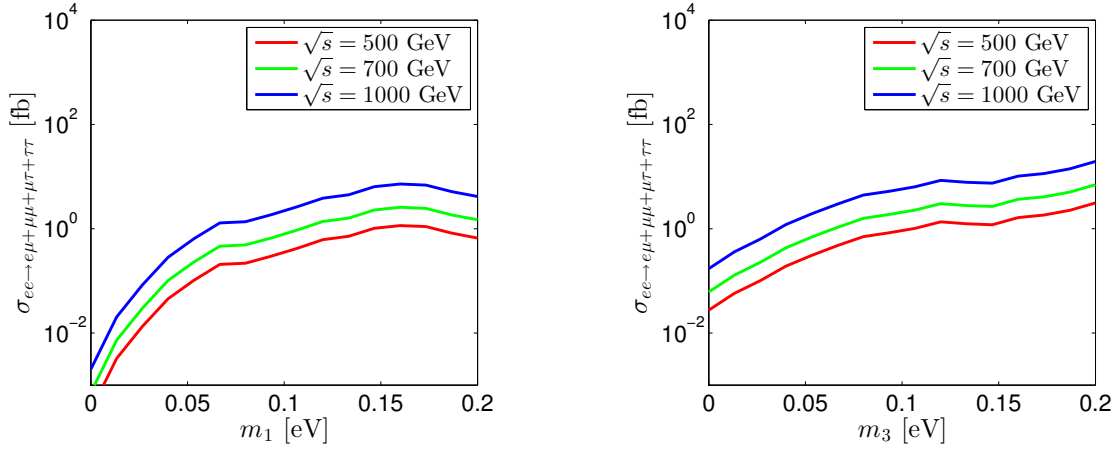


FIG. 6: Upper limits on the sum of the cross sections $\sigma(e^-e^- \rightarrow \mu^- \mu^-) + \sigma(e^-e^- \rightarrow \mu^- e^-) + \sigma(e^-e^- \rightarrow \mu^- \tau^-) + \sigma(e^-e^- \rightarrow \tau^- \tau^-)$ in the Higgs triplet model as a function of the lightest neutrino mass for center of mass energies $\sqrt{s} = 500, 700, 1000$ GeV. The doubly charged scalar mass is set to 2 TeV. The left (right) panel corresponds to normal (inverted) neutrino mass ordering.

model. Note also that even for large neutrino masses no relevant lower bound on the cross section can be derived in the triplet model, since Yukawa couplings can be made very small by increasing the VEV of the triplet above the keV range (up to the GeV scale).

B. Flavour structure of the Yukawa couplings

Let us now assume that either a leptonically decaying doubly charged resonance is found at LHC or a linear collider, or that lepton flavour violating processes $e^-e^- \rightarrow \alpha^- \beta^-$ are seen at a like-sign linear collider. In such a case the flavour structure of the decays or the LFV processes will be rather different in the two cases. Note that ratios of decay rates and LFV cross sections will be the same and proportional to the corresponding Yukawa couplings:

$$R_{\alpha_2 \beta_2}^{\alpha_1 \beta_1} \equiv \frac{\Gamma(k^{++} \rightarrow \alpha_1^+ \beta_1^+)}{\Gamma(k^{++} \rightarrow \alpha_2^+ \beta_2^+)} = \frac{\sigma(e^-e^- \rightarrow \alpha_1^- \beta_1^-)}{\sigma(e^-e^- \rightarrow \alpha_2^- \beta_2^-)} \quad (28)$$

where in the Zee–Babu model we have

$$R_{\alpha_2 \beta_2}^{\alpha_1 \beta_1} = \frac{(1 + \delta_{\alpha_1 \beta_1}) |g_{\alpha_1 \beta_1}|^2}{(1 + \delta_{\alpha_2 \beta_2}) |g_{\alpha_2 \beta_2}|^2}, \quad (29)$$

and in the triplet model an analogous relation holds but replacing the Yukawa coupling g by h . The important observation is that the flavour structure of those couplings will be rather different in the two models, with $h_{\alpha\beta}$ proportional to the neutrino mass matrix $m_{\alpha\beta}^{(\nu)}$, while for $g_{\alpha\beta}$ the relation to the neutrino mass matrix is more complicated.

We illustrate in Fig. 7 the cross section ratios of the LFV processes (or equivalently decay branching fractions) in the two models. For the sake of definiteness, all

the scalar masses are taken to be 3 TeV. Those results depend only weakly on the scalar masses. The different flavour structure of the two models can be clearly seen from the plots. In particular, in the Zee–Babu model, the dominating decay mode is always the $\mu\mu$ channel, no matter of the neutrino mass ordering. An observation of a significant fraction of events different from the di-muon channel would exclude the model. The largest contribution of a different flavour combination may occur for IO with a fraction of $\mu\tau$ events with $R_{\mu\mu}^{\mu\tau} \lesssim 0.2$.

In order to see this point more clearly, we insert the neutrino mixing parameters into Eq. (11) and obtain for the NO case

$$\begin{aligned} \zeta f_{\mu\tau}^2 \omega_{\mu\mu} &\simeq m_{33}^{(\nu)} \simeq m_3 c_{23}^2, \\ \zeta f_{\mu\tau}^2 \omega_{\mu\tau} &\simeq -m_{23}^{(\nu)} \simeq -m_3 s_{23} c_{23}, \\ \zeta f_{\mu\tau}^2 \omega_{\tau\tau} &\simeq m_{22}^{(\nu)} \simeq m_3 s_{23}^2, \end{aligned} \quad (30)$$

where $\omega_{\alpha\beta} = g_{\alpha\beta} m_{\alpha} m_{\beta}$ (defined after Eq. (11)) and terms proportional to the small parameters s_{13} , m_2 , and m_e have been neglected. Therefore, one has approximately $|\omega_{\mu\mu}| \simeq |\omega_{\mu\tau}| \simeq |\omega_{\tau\tau}|$ for a nearly maximal θ_{23} , and the ratios between Yukawa couplings are

$$g_{\mu\mu} : g_{\mu\tau} : g_{\tau\tau} \sim 1 : \frac{m_{\mu}}{m_{\tau}} : \frac{m_{\mu}^2}{m_{\tau}^2}. \quad (31)$$

Since the branching ratios are proportional to $|g_{\alpha\beta}|^2$, one finds $R_{\mu\mu}^{\tau\tau} \simeq m_{\mu}^4/m_{\tau}^4 \approx 10^{-5}$ and $R_{\mu\mu}^{\mu\tau} \simeq m_{\mu}^2/m_{\tau}^2 \approx 3 \times 10^{-3}$, in good agreement with the left plot of Fig. 7. Using the first line in Eq. (30) with $m_3 = \sqrt{\Delta m_{31}^2} \approx 0.05$ eV, one finds that $g_{\mu\mu}$ is bounded from below by neutrino masses [13]. Numerically we find

$$|g_{\mu\mu}| |f_{\mu\tau}|^2 \gtrsim 10^{-3} \frac{m_h \max(m_k, m_h)}{\mu \text{TeV}} \quad (\text{NO}). \quad (32)$$

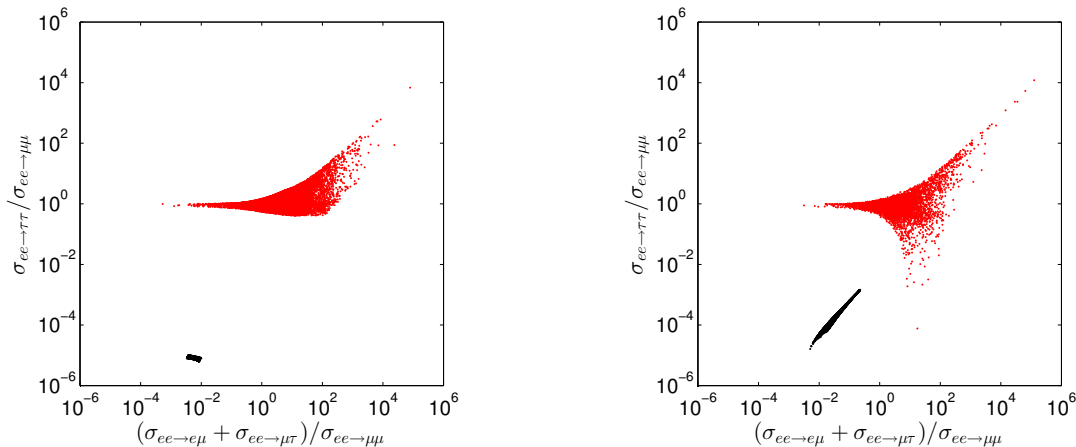


FIG. 7: Cross section ratios for processes $e^-e^- \rightarrow \ell_\alpha^- \ell_\beta^-$ (or equivalently ratios of branching fractions of the doubly charged scalar decays). The left (right) panel corresponds to normal (inverted) neutrino mass ordering. Black points denote the ratios in the Zee–Babu model, while red points correspond to the ratios in the Higgs triplet model. All scalar masses are taken to be 3 TeV. For the triplet model we vary the Majorana phases, the lightest neutrino mass between zero and 0.2 eV, and the triplet VEV between 0.1 eV and 1 keV.

Taking all the scalar masses to be 3 TeV as an example, the above condition indicates $|g_{\mu\mu}| \gtrsim 0.3$, where we have used Eq. (7) and the constraint from $\mu \rightarrow e\gamma$ on $f_{\mu\tau}$ from Tab. I. This lower bound on $g_{\mu\mu}$ is in good agreement with our numerical results.

In the case of IO the ratios in Eq. (31) hold only approximately. Because of the relations in Eq. (10), cancellations between the various terms in Eq. (11) become possible, leading to the correlation visible in the right panel of Fig. 7. We have checked numerically that for IO the lower bound corresponding to Eq. (32) is one order of magnitude weaker. Numerically we obtain a lower bound of $|g_{\mu\mu}| \gtrsim 0.1$ for scalar masses of 3 TeV, which can be understood by using Eq. (10) and the bound on $f_{e\mu}$ from CKM unitarity shown in Tab. I.

Finally, the g_{ee} contribution to the neutrino masses is strongly suppressed by the electron mass, and thus is allowed to be relatively sizeable compared to other Yukawa couplings. In the case that $g_{\mu\mu}$ lies close to its lower bound, the dominating decay channel could be ee instead of $\mu\mu$. The most interesting channels are then the $\mu\mu$ and ee channels. Note however, that this channel is not observable at the like-sign collider due to the Standard Model Møller scattering background. Hence this signature can only be explored if decays of an on-shell doubly charged scalar are observed.

C. Further different signatures

Apart from exploring the flavour structure of Yukawas there are several different signatures to distinguish the two models. In particular, for the triplet model there is large literature on additional observables. Below we give a brief review of a few possibilities.

Starting with collider signatures, we note that observing a doubly charged resonance below the lower bounds in the Zee–Babu model (Eqs. (24) or (25)) would favour the Higgs triplet. In such a case exploring the flavour structure of the decays (as illustrated in Fig. 7) may be used to establish the relation to neutrino mass, see for instance [50]. If a resonance is observed consistent with the Zee–Babu bounds, one may also look for the singly charged scalar, which is predicted in both models. In the triplet model the mass difference between the singly and doubly charged scalars is given by the VEV of the Higgs doublet, v , times a dimensionless coupling in the scalar potential. Therefore, generically one expects a mass difference $\lesssim v$. In the Zee–Babu model the two scalar masses are unrelated. Moreover, the triplet couples to W^\pm , which allows processes like for instance $H^+ \rightarrow H^{++}W^-$. Signatures of the singly charged triplet component have been investigated in [51–54].

Another difference of the models is that the doubly charged scalar in the Zee–Babu model (triplet model) couples to right-handed (left-handed) leptons. In the case of LFV processes at a like-sign linear collider one can use the polarization of the beams to find out the chirality structure of the effective operator induced by the heavy doubly charged scalar [45]. The possibility to determine the chirality at a hadron collider by using tau decays has been investigated in [55].

Apart from collider experiments, measurement sensitive to the absolute neutrino mass scale will be important, see [56] for a recent review. Since the Zee–Babu model predicts the lightest neutrino mass to be zero, it can be ruled out by establishing a non-zero lightest neutrino mass for instance in neutrinoless double beta decay experiments, kinematical neutrino mass measurement, and/or in cosmology, eventually combined with a

determination of the neutrino mass ordering from oscillation experiments [57].

VII. CONCLUSIONS

We have studied the current experimental constraints on the Zee–Babu model, taking into account recent data on lepton mixing angles and the MEG limit on $\mu \rightarrow e\gamma$. By performing a numerical parameter scan of the model we find that most likely the charged scalars of the Zee–Babu model will be out of reach for the Large Hadron Collider (LHC), including the 14 TeV configuration. If a signal should indeed be seen at LHC this would push the model into a fine tuned parameter region close to the limit of perturbativity. In such a case a signal in upcoming experiments searching for charged lepton flavour violation, such as $\mu \rightarrow e$ conversion on nuclei or $\mu \rightarrow e\gamma$ is guaranteed.

Even if the doubly charged scalar of the model is too heavy to be produced at a collider we point out that a sub-TeV linear collider operated in the like-sign mode may reveal lepton flavour violating processes $e^-e^- \rightarrow \alpha^-\beta^-$ due to contact interactions induced by the heavy doubly charged scalar. Assuming luminosities of several 10 fb^{-1} such processes might be observable for scalar masses up to 10 TeV. We stress however, that no signal can be guaranteed, since it is proportional to the Yukawa coupling g_{ee} which is essentially unconstrained by neutrino data.

Furthermore we have considered the same signature for an alternative model for neutrino mass, the Higgs triplet model, which has a similar particle spectrum as the Zee–

Babu model, although the mechanism of neutrino mass generation is very different. We have shown that those two models lead to a very different flavour structure of LFV signatures at a like-sign collider (or equivalently to ratios of branching fractions of doubly charged scalar decays, in case they are kinematically accessible). We have outlined various characteristic signatures of the two models. If neutrino mass should indeed be generated by one of those two extensions of the scalar sector it seems likely that the correct model can be identified by using an interplay of various collider signatures as well as absolute neutrino mass measurement.

Note: During the final stage of this work we became aware of Ref. [58] where also an updated parameter scan in the Zee–Babu model is performed. Taking into account the slightly different method to derive the allowed parameter region and different perturbativity and fine-tuning requirements our results are consistent.

Acknowledgment

We thank the authors of [58] for sharing their preliminary results with us. One of the authors (H.Z.) is indebted to Werner Rodejohann for useful discussions. This work was supported by the International Max Planck Research School for Precision Tests of Fundamental Symmetries (D.S.) and the Max Planck Society in the project MANITOP (H.Z.). T.S. acknowledges partial support from the European Union FP7 ITN INVISIBLES (Marie Curie Actions, PITN-GA-2011-289442).

-
- [1] Y. Farzan, S. Pascoli, and M. A. Schmidt, *JHEP* **03**, 107 (2013), 1208.2732.
 - [2] P. W. Angel, N. L. Rodd, and R. R. Volkas, *Phys. Rev. D* **87**, 073007 (2013), 1212.6111.
 - [3] S. S. C. Law and K. L. McDonald (2013), 1303.6384.
 - [4] W. Konetschny and W. Kummer, *Phys. Lett.* **B70**, 433 (1977).
 - [5] T. P. Cheng and L.-F. Li, *Phys. Rev.* **D22**, 2860 (1980).
 - [6] A. Zee, *Phys. Lett.* **B161**, 141 (1985).
 - [7] A. Zee, *Nucl. Phys.* **B264**, 99 (1986).
 - [8] K. S. Babu, *Phys. Lett.* **B203**, 132 (1988).
 - [9] M. Lindner, D. Schmidt, and T. Schwetz, *Phys. Lett.* **B705**, 324 (2011), 1105.4626.
 - [10] S. Baek, P. Ko, and E. Senaha (2012), 1209.1685.
 - [11] K. S. Babu and C. Macesanu, *Phys. Rev.* **D67**, 073010 (2003), hep-ph/0212058.
 - [12] D. Aristizabal Sierra and M. Hirsch, *JHEP* **12**, 052 (2006), hep-ph/0609307.
 - [13] M. Nebot, J. F. Oliver, D. Palao, and A. Santamaria, *Phys. Rev.* **D77**, 093013 (2008), arXiv:0711.0483.
 - [14] T. Ohlsson, T. Schwetz, and H. Zhang, *Phys. Lett.* **B681**, 269 (2009), 0909.0455.
 - [15] Y. Abe et al. (DOUBLE-CHOOZ Collaboration), *Phys. Rev. Lett.* **108**, 131801 (2012), 1112.6353.
 - [16] F. An et al. (DAYA-BAY Collaboration), *Phys. Rev. Lett.* **108**, 171803 (2012), 1203.1669.
 - [17] J. Ahn et al. (RENO collaboration), *Phys. Rev. Lett.* **108**, 191802 (2012), 1204.0626.
 - [18] M. Gonzalez-Garcia, M. Maltoni, J. Salvado, and T. Schwetz, *JHEP* **1212**, 123 (2012), www.nu-fit.org, 1209.3023.
 - [19] J. Adam et al. (MEG Collaboration) (2013), 1303.0754.
 - [20] J. Schechter and J. W. F. Valle, *Phys. Rev.* **D22**, 2227 (1980).
 - [21] G. Lazarides, Q. Shafi, and C. Wetterich, *Nucl. Phys.* **B181**, 287 (1981).
 - [22] R. N. Mohapatra and G. Senjanović, *Phys. Rev.* **D23**, 165 (1981).
 - [23] D. Chang, W.-Y. Keung, and P. Pal, *Phys. Rev. Lett.* **61**, 2420 (1988).
 - [24] K. L. McDonald and B. H. J. McKellar (2003), hep-ph/0309270.
 - [25] R. Kitano, M. Koike, and Y. Okada, *Phys. Rev.* **D66**, 096002 (2002), hep-ph/0203110.
 - [26] D. Dinh, A. Ibarra, E. Molinaro, and S. Petcov, *JHEP* **1208**, 125 (2012), 1205.4671.

- [27] E. Ma, M. Raidal, and U. Sarkar, Nucl. Phys. **B615**, 313 (2001), hep-ph/0012101.
- [28] J. Beringer et al. (Particle Data Group), Phys. Rev. **D86**, 010001 (2012).
- [29] G. Bennett et al. (Muon G-2 Collaboration), Phys. Rev. **D73**, 072003 (2006), hep-ex/0602035.
- [30] U. Bellgardt et al. (SINDRUM Collaboration), Nucl. Phys. **B299**, 1 (1988).
- [31] K. Hayasaka, K. Inami, Y. Miyazaki, K. Arinstein, V. Aulchenko, et al. (Belle Collaboration), Phys. Lett. **B687**, 139 (2010), 1001.3221.
- [32] B. Aubert et al. (BaBar Collaboration), Phys. Rev. Lett. **104**, 021802 (2010), 0908.2381.
- [33] W. H. Bertl et al. (SINDRUM II Collaboration), Eur. Phys. J. **C47**, 337 (2006).
- [34] R. Abrams et al. (Mu2e Collaboration) (2012), 1211.7019.
- [35] K. Knoepfel et al. (R. C. Group) (2013), 1307.1168.
- [36] Y. Cui et al. (COMET Collaboration) (2009), KEK-2009-10.
- [37] H. Witte, B. Muratori, K. Hock, R. Appleby, H. Owen, et al., Conf. Proc. **C1205201**, 79 (2012).
- [38] F. del Aguila, M. Chala, A. Santamaria, and J. Wudka, Phys. Lett. **B725**, 310 (2013), 1305.3904.
- [39] A. Alloul, M. Frank, B. Fuks, and M. R. de Traubenberg, Phys. Rev. **D88**, 075004 (2013), 1307.1711.
- [40] G. Aad et al. (ATLAS Collaboration), Eur. Phys. J. **C72**, 2244 (2012), 1210.5070.
- [41] S. Chatrchyan et al. (CMS Collaboration), Eur. Phys. J. **C72**, 2189 (2012), 1207.2666.
- [42] T. G. Rizzo, Phys. Rev. **D25**, 1355 (1982).
- [43] T. G. Rizzo, Phys. Lett. **B116**, 23 (1982).
- [44] D. London, G. Belanger, and J. Ng, Phys. Lett. **B188**, 155 (1987).
- [45] F. Cuyppers and M. Raidal, Nucl. Phys. **B501**, 3 (1997), hep-ph/9704224.
- [46] M. Raidal, Phys. Rev. **D57**, 2013 (1998), hep-ph/9706279.
- [47] O. Cakir, New J. Phys. **8**, 145 (2006), hep-ph/0604183.
- [48] W. Rodejohann, Phys. Rev. **D81**, 114001 (2010), 1005.2854.
- [49] W. Rodejohann and H. Zhang, Phys. Rev. **D83**, 073005 (2011), 1011.3606.
- [50] J. Garayoa and T. Schwetz, JHEP **0803**, 009 (2008), 0712.1453.
- [51] P. Fileviez Perez, T. Han, G.-y. Huang, T. Li, and K. Wang, Phys. Rev. **D78**, 015018 (2008), 0805.3536.
- [52] A. Akeroyd and C.-W. Chiang, Phys. Rev. **D80**, 113010 (2009), 0909.4419.
- [53] M. Aoki, S. Kanemura, and K. Yagyu, Phys. Rev. **D85**, 055007 (2012), 1110.4625.
- [54] A. Akeroyd and H. Sugiyama, Phys. Rev. **D84**, 035010 (2011), 1105.2209.
- [55] H. Sugiyama, K. Tsumura, and H. Yokoya, Phys. Lett. **B717**, 229 (2012), 1207.0179.
- [56] C. Weinheimer and K. Zuber, Annalen der Physik, **525**, 565 (2013), 1307.3518.
- [57] M. Blennow, P. Coloma, P. Huber, and T. Schwetz (2013), 1311.1822.
- [58] J. Herrero-Garcia, M. Nebot, N. Rius, and A. Santamaria (2014), to appear.